Wing-In-Ground Effect on Free Surface

Yong Hwan Kim[1], Shin-Hyung Rhee[1] and Sang-Min Jee[1]

[1] Department of Naval Architecture and Ocean Engineering, Seoul National University, Seoul, Korea;
Corresponding Author: yhwangkim@snu.ac.kr

Abstract

This study aims the observation of wing-in-ground effect near free surface. Numerical computations are carried out to observe the deformation of free surface and the effects on lift and drag. The detailed flow fields around two- and three-dimensional wings with NACA 0012 section are observed from the results of a commercial CFD program, FLUENT, and the local deformations of free surface are obtained by applying a Rankine panel method. In the present cases, the small deformation of free surface under the wings is observed, but different forces are found between solid wall and free surface when the speed of wings becomes large.
Keywords: wing-in-ground effect, WIG craft, pressure-patch problem

1 Introduction

WIG crafts (Wingship, Ekranoplan) utilize the ground effect of lift, known to occur when the gap between wing trail and ground is less than 30% of chord length. This type of craft is recently of great interest in Asian countries due to the growth of trading market and the demand of fast transportation. A good summary about the WIG craft can be found in the technical report of ARPA (1994).

In the present study, the effect of free surface on the lift and drag of flying WIG crafts is considered. There are two primary interests when the effect of free surface is concerned: the deformation of free surface, and non-flat wavy profile. The present study focuses on the former issue.

All the experimental observations on the lift and drag on wings flying closely over ground have been carried out in wind tunnels which have solid ground. In actual flying situations, the ground is not solid boundary but free surface. There is no doubt that there is difference of hydrodynamic forces between the wings flying over solid wall and free surface, but some numerical studies, e.g. Barber (1998, 2004), showed that the deformation of overall free surface is not significant. This, however, may not imply that the hydrodynamic forces are the same. Since lift is very sensitive to the clearance between wing and ground, i.e. the height of flying wing, a small change of free surface elevation may cause a non-ignorable difference of lift.

This study intends to observe the deformation of free surface near a wing in ground, and the hydrodynamic forces for different ground conditions. To this end, two numerical

approaches are applied for two- and three-dimensional wings of NACA0012 section, flying over solid wall and free surface. At first, a commercial program, FLUENT, is used to get the numerical solution of the Navier-Stokes equation around the wings. The detailed flow fields in different Froude numbers and ground conditions are obtained, and lifts and drags are compared. To observe the effect of air pressure around the wings on the deformation of free surface, a Rankine panel method is adopted. In this computation, the pressure-patch problem is solved for different but given pressure fields. .

In the present study, the deformations of free surface profile around the wings in ground are found insignificant, as predicted. However, some difference of hydrodynamic coefficients is found.

2 Wing in solid ground and free surface

Consider a wing flying closely over ground with a steady speed, as shown in Figure 1. Force on the wing depends on flying height, *h*, and the profile of the ground. In this case, two particular cases of the ground are considered: solid wall and free surface.
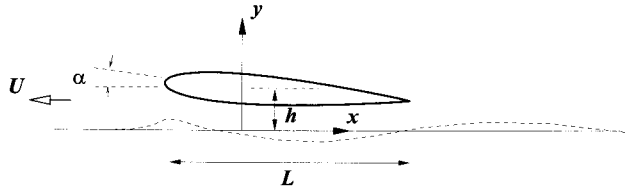

Figure 1: Wing in ground: Coordinate system

For the solid ground, the boundary value problem becomes relatively easier than the case of free surface. No-flux condition with free slip or no slip is enough on the ground. When the ground is free surface, boundary condition becomes more complicated. To observe this case, let's assume that potential flows are valid in fluid flows. Particularly, in the linear regime, the free-surface boundary condition can be written as follows:

$$\frac{\partial^2 \varphi}{\partial x'^2} + \frac{g}{U^2}\frac{\partial \varphi}{\partial y} = 0 \tag{1}$$

where x' is the x coordinate of x-axis in moving frame, i.e. $x' = x - Ut$. It is interesting to consider two limit cases of the linear free surface boundary condition:

$$- \; U \rightarrow 0 : \; \frac{\partial \varphi}{\partial y} = 0 \tag{2}$$

$$- \; U \rightarrow \infty : \; \varphi = 0 \tag{3}$$

The first case indicates that the free surface behaviours like solid wall. On the other hand, the second becomes pressure-release problem. The difference of two problems can be described with point images, as shown in Figure 2. It is obvious that the flow fields and the corresponding lift and drag forces can be different, which strongly depend on the advancing speed and height of the wing, i.e. *U* and *h*. A physical difference of these two cases owes to the deformation of free surface. Due to air pressure acting on free surface

around the wing, there is the deformation of free surface around the wing. Then flow field becomes not the same to that of solid ground. Such deformation requires energy input by the wing, causing the reduction of lift.
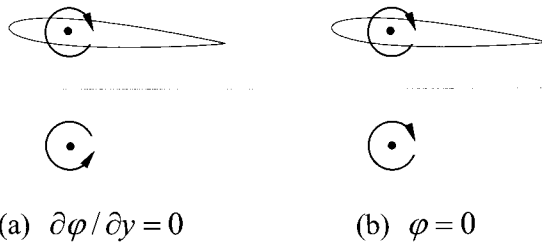

(a) $\partial\varphi/\partial y = 0$ (b) $\varphi = 0$

Figure 2: Differences of two limit cases

For the design of a WIG craft, the second case should be considered to predict the lift on wings. However, the performance prediction of wing in ground for the WIG design has been mostly relied on experiment in wind tunnel which the ground is solid. Figure 3 shows an example of force and moment curves for a WIG configuration wind tunnel test (from ARPA report, taken from Reeves 1993). As this figure shows, when the clearance between wing and ground is small, the variation of lift becomes very sensitive to the clearance height. Therefore, it is important to check the degree of free-surface deformation near wing and the change of lift. Then the design condition may be changed.
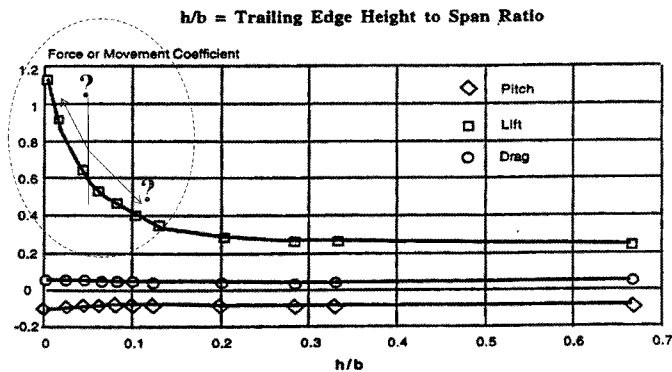

Figure 3: Force and moment coefficient variation due to WIG effect (taken from Reeves 1993)

2 Numerical methods

The present study applies two numerical methods to observe the effect of free surface on a wing in ground and the deformation of free surface. A commercial CFD program, FLUENT, is used to obtain the detailed flow information around the wing, and a Rankine panel method is applied to compute wave elevation around pressure patches imitating the wing.

2.1 Navier-stokes equation solver: FLUENT

The governing equations are written for the mass and momentum conservation, such that

$$\frac{\partial \rho}{\partial t} + \nabla \cdot \left(\rho \vec{v} \right) = 0 \tag{4}$$

$$\frac{\partial}{\partial t} \left(\rho \vec{v} \right) + \nabla \cdot \left(\rho \vec{v} \vec{v} \right) = -\nabla p + \nabla \cdot \left(\overline{\overline{\tau}} \right) \tag{5}$$

where $\vec{v}$ is the velocity vector in the Cartesian coordinate system, p the static pressure, and τ the stress.

Once the Reynolds averaging approach for turbulence modeling is applied, the Navier-Stokes equations can be written in Cartesian tensor form as

$$\frac{\partial \rho}{\partial t} + \frac{\partial}{\partial x_i} \left(\rho u_i \right) = 0 \tag{7}$$

$$\frac{\partial}{\partial t} \left(\rho u_i \right) + \frac{\partial}{\partial x_j} \left(\rho u_i u_j \right) = -\frac{\partial p}{\partial x_i} +$$

$$\frac{\partial}{\partial x_j} \left[\mu \left(\frac{\partial u_i}{\partial x_j} + \frac{\partial u_j}{\partial x_i} - \frac{2}{3} \delta_{ij} \frac{\partial u_l}{\partial x_l} \right) \right] + \frac{\partial}{\partial x_j} \left(-\rho \overline{u_i' u_j'} \right)_i \tag{8}$$

where δ_{ij} is the Kronecker delta, and $-\rho \overline{u_i' u_j'}$ the Reynolds stresses. The Reynolds stress term is related to the mean velocity gradients, i.e., turbulence closure, by the Boussinesq hypothesis. The Reynolds stresses are modeled using the shear-stress-transport k-ω model, SST-KO hereafter. The SST-KO (Menter, 1994) is essentially a zonal model which blends a modified version of the Wilcox' k-ω model in the inner layer and a k-ω model derived from the standard k-ε model in the outer layer.

The VOF method was employed to handle the free-surface wave flow around a surface-piercing structure. The VOF formulation relies on the fact that two or more fluids/phases are not interpenetrating. A single momentum equation is solved throughout the domain, and the resulting velocity field is shared among the phases. The momentum equation depends on the volume fractions of all phases through the fluid properties, which are determined by the presence of the component phases in each cell.

For the calculation of face fluxes for the VOF model, the high-resolution interface capturing (HRIC) scheme is used. Two modifications were applied to the original HRIC scheme such that (1) the explicit integration of the volume fraction equation is done within a sub-iteration loop with a prescribed value of Courant number, and (2) instead of using first order upwind discretization, the one-dimensional bounded version of QUICK (Leonard, 1979) is used, when the flow is parallel to the interface.

2.2 Rankine panel method: pressure-patch problem

A Rankine panel method is applied for observing the deformation of free surface due to the wing-in-ground effect. Local air pressures around the wing, predicted by FLUENT, are imposed on free surface, and the generated waves are obtained by the Rankine panel method. This is a pressure-patch problem, not the same to the actual lifting problem, but the degree of free-surface deformation can be observed by this way.
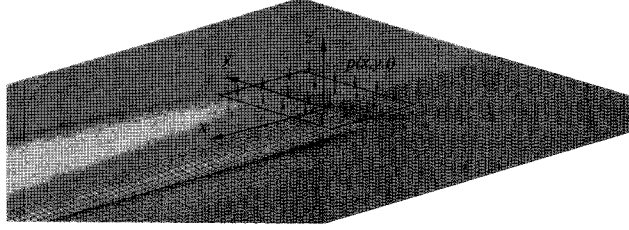
Figure 4: Pressure-patch problem

This study focuses on the linear problem with the free-surface boundary conditions that take the following form (see Figure 4):

$$\frac{\partial \varphi}{\partial t} + g\eta + \frac{p}{\rho} = -\frac{1}{2}U^2, \quad \frac{\partial \eta}{\partial t} - \frac{\partial \varphi}{\partial z} = 0 \qquad (12, 13)$$

where $\varphi(x,y,z,t)$ is the disturbance potential due to a advancing pressure patch $p(x,y,t)$ and $\eta(x,y,t)$ indicates wave elevation. The total potential is $\Phi(x,y,z,,t) = Ux + \varphi(x,y,z,t)$. As a matter of fact, a steady-flow formulation is valid for the present problem, but an unsteady approach is considered for future use.

The boundary of fluid domain is discretized into quadrilateral panels, and the physical variables are represented with a higher-order B-spline basis function. The velocity potential adopts the representation,

$$\phi(\vec{x}_i, t) \approx \sum_j \phi_j(t) B_j(\vec{x}_i) =$$
$$\sum_j \phi_j(t) \, b^{(p)}(\xi_1; \vec{x}_i) b^{(q)}(\xi_2, \vec{x}_i) \qquad (14)$$

where $B_j(\vec{x}_i)$ is the B-spline basis function of order $(p.q)$, defined relative to the local panel coordinates (ξ_1, ξ_2). The same approximation is applied to the wave elevation and normal velocity over the fluid boundaries.

There are three unknown parameters: potential, elevation, and normal velocity on the free surface. These can be obtained by solving three equations –Green's 2nd identity, kinematic and dynamic free-surface boundary conditions- explicitly and implicitly.

$$(\varphi)_j^{n+1} B_{ij} + (\varphi)_j^{n+1} \iint_S B_{ij}(\vec{\xi}) \frac{\partial}{\partial n} G(\vec{x}; \vec{\xi}) d\xi$$
$$- (\frac{\partial \varphi}{\partial n})_j^{n+1} \iint_S B_{ij}(\vec{\xi}) G(\vec{x}; \vec{\xi}) d\xi = 0 \qquad (15)$$

$$\frac{(\eta)_j^{n+1} - (\eta)_j^n}{\Delta t} = Q(\varphi^n, \eta^n, ...) \qquad (16)$$

$$\frac{(\varphi)_j^{n+1} - (\varphi)_j^n}{\Delta t} = R(\varphi^n, \eta^{n+1}, ...) \qquad (17)$$

Q and R are the forcing terms, which are defined in equations (13) and (14). It should be noted that the wave elevation obtained from equation (16) is used as input in equation (17). Combining equations (16) and (17) with the boundary integral equation (15), allows the values of the velocity potentials and the normal velocities on the free surface to be updated.

The pressure patch $p(x, y, t)$ can have any type of distribution. In the present computation, the result of FLUENT is applied. In particular, the non-zero pressure is assumed only near the wing. Therefore wave profiles are different with the results of FLUENT.

3 Numerical computation & results

Computational effort is concentrated on 2D and 3D wings with NACA 0012 section. In the case of the 3D wings, the same span length is same to chord length, and an end-plat with zero-thickness is attached at each end of span. The height of the wing center from the ground is $0.12L$ where L is chord length, and the angle of attack is set to be 4 degrees. Then the clearance between the ground and trailing edge is about $0.0677L$.

Figure 5 presents the partial views of the 3D grid for the problem with free-surface effect. To ensure the high quality grid and also to exploit the simplicity of the geometry, multi-block structured grids were generated for the problem without free-surface wave effect. The cell counts for the 2D and 3D grids are 10,800 and 461,960, respectively. The same grids were extended to the underwater region for the problem with free-surface effect, in such a way that the depth of 2.5 times the chord length was ensured. The cell counts for these extended 2D and 3D grids are 24,444 and 1,007,720, respectively. Note that the 3D grids were generated by extruding the 2D grids in the third direction.
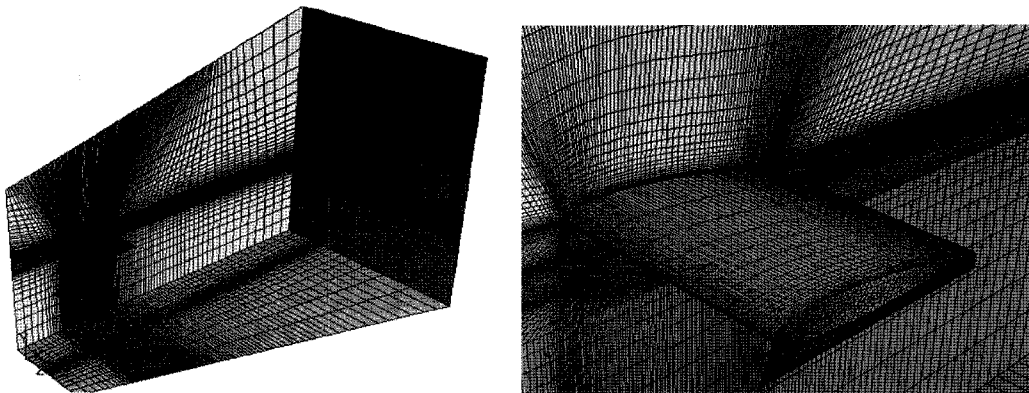
(a) Grids in computational domain   (b) Grids around 3D wing

Figure 5: Solution grids for 3D wing with end-plat

Lift and drag are observed at four speeds, and the results are summarized in Table 1. The lift coefficient of 2D NACA0012 foil in unbounded fluid is about 0.44 in a wide range of the Raynolds number (e.g. Sheldahl et al. 1981), while the present computation provides 0.439 in the fluid region bounded by solid ground. In fact, two quantities are not necessary to be the same since the WIG effect is involved, also not needed to be dramatically large since the increase/decrease depends on wing section and the angle of attack. A more

thorough investigation is needed for this issue, but our interest in this study focuses on the difference due to ground condition.

Table 1: Lift and drag coefficients

Fr (Rn)	2/3D	Ground	C_L	C_D
0.64 (1.4 x10⁵)	2D	Solid	0.439	0.021
		F.S.	0.427	0.022
	3D	Solid	0.367	0.026
		F.S.	0.361	0.029
1.60 (3.6 x10⁵)	2D	Solid	0.466	0.020
		F.S.	0.460	0.020
	3D	Solid	0.387	0.025
		F.S.	0.374	0.027
2.0 (4.5 x10⁵)	2D	Solid	0.459	0.018
		F.S.	0.420	0.018
3.0 (6.8 x10⁵)	2D	Solid	0.449	0.016
		F.S.	0.412	0.015

(Fr: Froude number, Rn: Reynolds number)
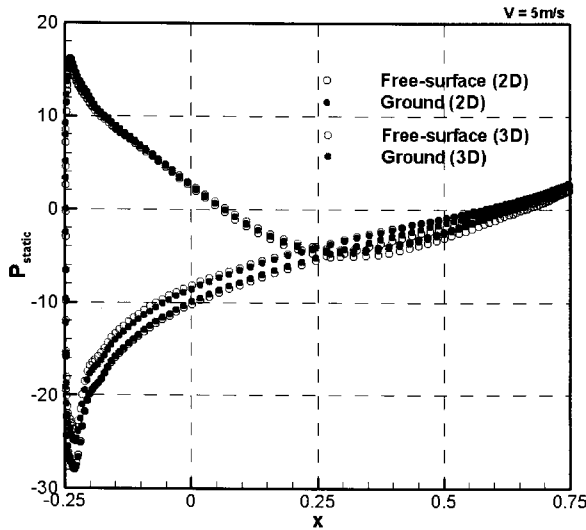
Figure 6: Surface pressure distribution at Fr=1.6: mid span location for 3D case

At the speed of Froude number 0.64 and 1.6, in general, the free-surface effect is not significant, and difference is only a few percent. Except for the region very close to the end fin, the surface pressure distribution and free-surface variation in the 2D case is very similar to that of 3D wing's cross sections (see Figure 6~8). However, the drag values show slightly larger difference, suggesting the energy taken out due to the wave generation, although not very large.

At Fn=2.0 and 3.0, the influence of free-surface wave become more significant, and the decrease of lift coefficient becomes not ignorable. This amount of change should be taken into account in the design of a WIG craft.

Figure10 shows the profile of free surface in the 2D cases. The length scale is normalized with respect to chord length. Yet the deformation of free surface is not significant, but this amount of deformation may cause not small reduction of lift due to the energy loss to generate water waves.
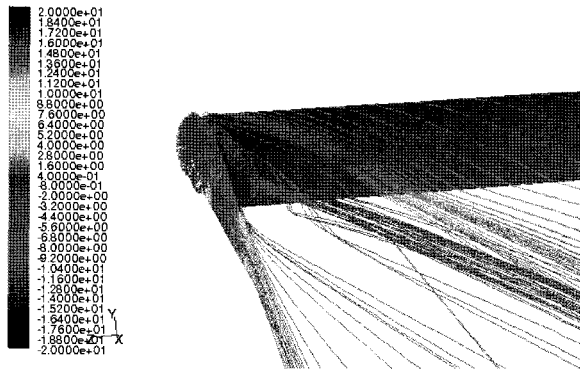
Figure 7: Pathlines around the wing tip and end fin in 3D case: Fr=1.6
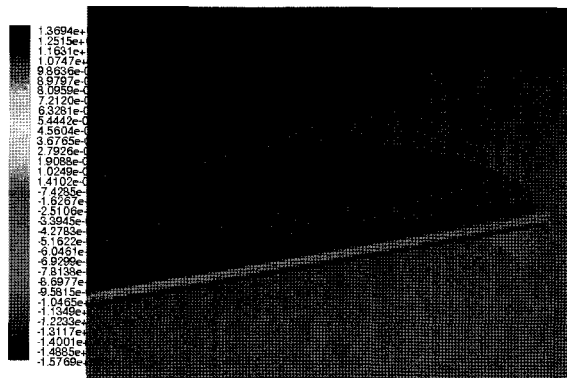
Figure 8: Surface pressure coefficient contours around wing tip and end fin in 3D case: Fr=1.6
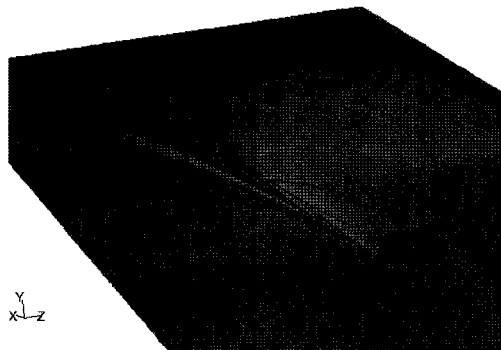
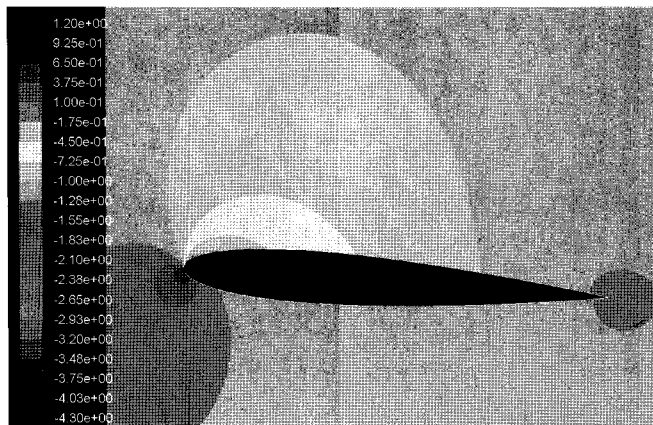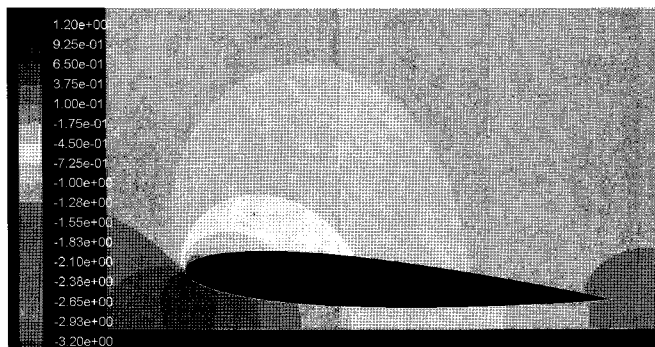**Figure 9:** Wave contours around 3D wing: Fr=1.6
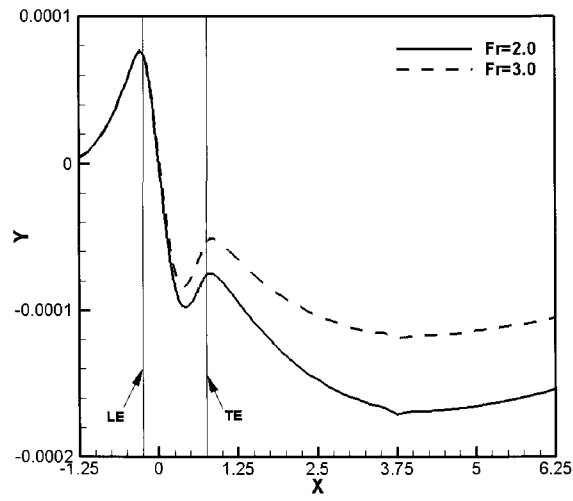
Figure 10: Free-surface wave profile in 2D cases

(a) Unbounded domain

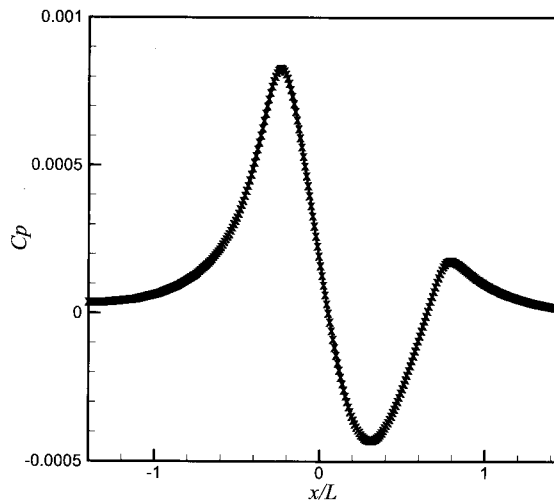(b) With ground

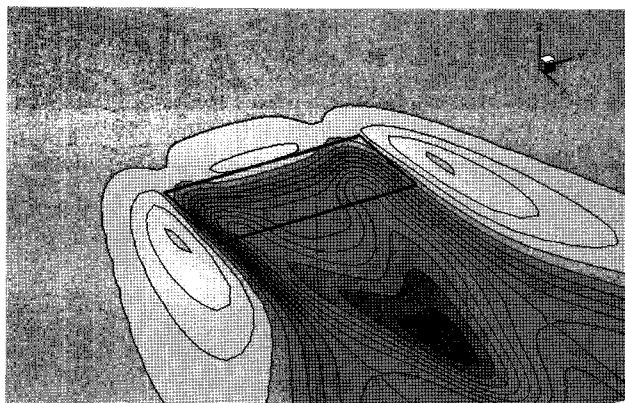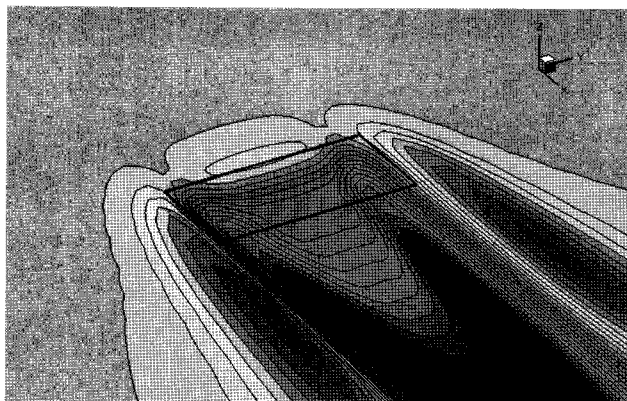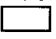**Figure 11:** Pressure contours around the wing: Fn=3.0

Figure 12: Pressure coefficients on free surface for pressure patch: The wing is in the range of $x/L=-0.25\sim0.75$(The coefficient is normalized with respect to water density.)

(a) Fn=2.0

(b) Fn=4.0

Figure 13: Contour of wave elevation around pressure patch at Fn=2.0 (top) and 4.0 (bottom): ☐ represents wing profile.

(a) at leading edge

(b) at wing center

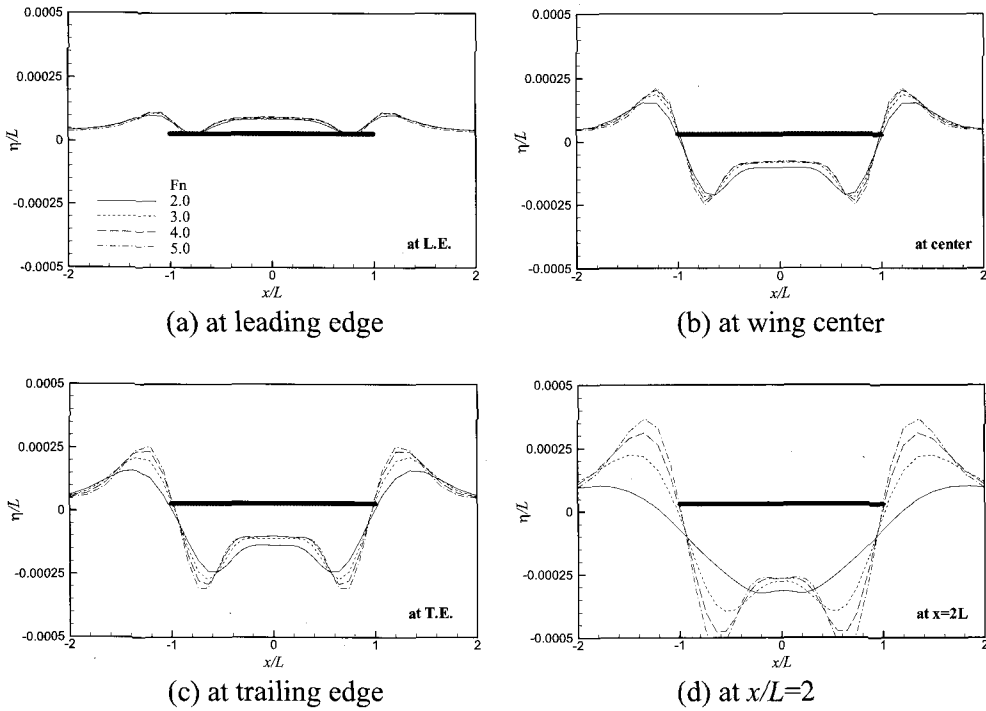(c) at trailing edge

(d) at $x/L=2$

Figure 14: Sectional profile of free surface at different locations: solid line for pressure patch
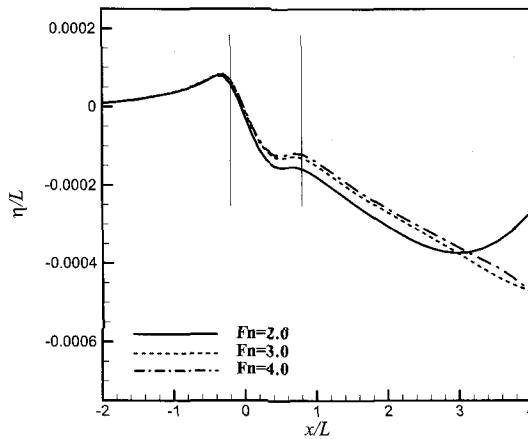

Figure 15: Wave profiles at $y=0$: L.E. at $x=-0.25$, T.E. at $x=0.75$

Figure 13 shows the wave contours around the pressure patch at two Froude numbers, 2.0 and 4.0, and Figure 14 shows the sectional profiles of free surface elevation at several speeds. Moreover, the centerline profile of wave elevation is shown in Figure 15.

According to these results, despite the difference of speed, the wave elevation near leading edge does not vary much for different speed. This is consistent with the result of the FLENT computation, shown in 10. However, the dependency on the speed at downstream behind trailing edge is significant because of not only pressure difference but also dispersion property. The wave elevations below the wing, obtained by FLUENT and

Rankine panel methods, are in a fair agreement at Fn=2.0 and 3.0, but it is found that the discrepancy at downstream is obvious. Particularly, wave troughs predicted by Rankine panel method are much deeper than those of FLUENT.

4 Conclusions

In the present paper, two numerical methods are applied to observe the deformation of free surface elevation cased by wing-in-ground effect, and the effects on hydrodynamic forces. From the numerical results, it is found that the magnitude of wave elevation is not large at the speed range considered in this study. Despite small deformation of elevation, however, some difference of lift is observed at high speed. It is also observed that wave profile just below the wing is not much sensitive to speed at high Froude number, but stronger sensitivity is found in downstream.

References

Advanced Research Projects Agency(ARPA). 1994. Wingship Investigation, Final Report, **I, II, III**.

Barber, T., Leonardi, E. and Archer, D. 1998. Free Surface Deformation Caused by a Wing in Ground Effect over Water, Proceedings of International Workshop, WISE up to Ekranoplan GEMs, The University of New South Wales, Sydney, Australia, 90-101.

Barber, T. 2004. Free surface deformation Caused by a Moving wing in Ground Effect Flying over Water. International Maritime Conference, Syndey, Australia.

Chun, H. H. and I. R. Park. 1995. Analysis of Steady and University Performances for 3-D Airwings in the Vicinity of the Free Surface. Proc. International Workshop Ekranoplans-Flying Ships of the 21st Century, The University of New South Wales, 23-46.

Kataoka, K., J. Ando and K. Nakatake. 1992. Free Surface Effect on Characteristics of Two-Dimensional Wing. Transactions of the West-Japan Society of Naval Architects, **83**.

Leonard, B.P. 1979. A Stable and Accurate Convective Modeling Procedure Based on Quadratic Upstream Interpolation. Computer Methods in Applied Mechanics and Engineering, **19**, 59-98

Menter, F.R. 1994. Two-Equation Eddy-Viscosity Turbulence Models for Engineering Applications. AIAA Journal, **32, 8**, 1598 – 1605.

Muzaferija, S, M. Peric, P. Sames and T. Schellin. 1998. A Two-Fluid Navier-Stokes Solver to Simulate Water Entry. In: Proc 22nd Symposium on Naval Hydrodynamics, Washington, DC, 277-289.

Reeves, J.M.L. 1993. The Case for Surface Effect Research, Platforms and Technology Development Opportunities, NOTO AGARD Fluid Mechnanics Panel (FMP) Symposimum on Recent Advances in Long Range and Long Range Endurance Operation of Aircraft, 24-27.

Sheldahl, R.E. and P.C. Klimas. 1981. Aerodynamic Characteristics of Seven Airfoil Sections Through 180 Degrees Angle of Attack for Use in Aerodynamic Analysis of Vertical Axis Wind Turbines. SAND80-2114, Sandia National Laboratories, Albuquerque, New Mexico.